ESR dating of interfault gypsum from Katrol hill range, Kachchh, Gujarat: Implications for neotectonism

George Mathew[1,*], T. K. Gundu Rao[2], P. S. Sohoni[3] and R. V. Karanth[3]

[1]Department of Earth Sciences, and [2]Regional Sophisticated Instrumentation Centre, Indian Institute of Technology Bombay, Powai, Mumbai 400 076, India
[3]Department of Geology, M. S. University of Baroda, Vadodara 390 002, India

This article presents chronological investigations on interfault fibrous gypsum using the technique of Electron Spin Resonance (ESR) dating, essentially to demonstrate the robustness of the technique as a dating tool on fibrous gypsum precipitates in a semi-arid region. Samples of fibrous gypsum collected from Katrol hill range, Kachchh consist of those from fractures and bedding planes, and those along the inferred fault plane. The slow progressive uplift along the region resulted in erosion, unloading and dissolution of near-surface evaporite deposits and formation of extensional joints parallel to bedding and across. These openings became favourable sites for the fibrous gypsum to develop perpendicular to the wall of factures as well as fault plane. ESR chronometry studies deduce that gypsum growth along the bedding plane and fractures took place around 300 ka, while ESR dating studies on fault plane gypsum indicate an age around 70 ka. The young age of the normal fault plane indicates that it developed on account of the ongoing compressive stresses which resulted in normal faults perpendicular to the principal stress and later got immediately filled by sulphate-rich solutions. The ongoing compressive stresses active on the region have finally resulted in further uplift of the footwall back limb to its present topography.

CHRONOLOGY of a faulting activity is of vital importance in studies related to neotectonism. This is especially to determine the age of recent rupture and time intervals between different events, which are extremely important parameters in the earthquake hazard assessment of any region. In the absence of proper chronology of deposits, it is often difficult to determine the magnitude of tectonic activity of any region. Fault movements are dated by various methods such as: (a) fission track dating of epidote material along fault plane[1], (b) U-series dating of carnotite and tyuyamunite along fault plane[2], (c) Rb–Sr, K–Ar and tritium isotope technique on intrafault material,[3] and (d) luminescence dating[4]. It is, however, the robust Electron Spin Resonance (ESR) dating of fault gouge proposed by Ikeya *et al.*[5], that gained much wider acceptance worldwide. Each chronometric technique has its own advantages as well as limitations. Radiocarbon ages of soil layers that get deformed during faulting events provide approximately reliable ages of earthquake event, provided the carbon is not a transported matter. However, these methods are useful only where active faults are found to displace younger deposits from which datable carbon is extracted. In poor-to-moderate consolidated sediments in arid to semi-arid climates, occurrence of organic carbon is rather remote.

The most suitable material for ESR dating is the finely crushed gouge material resulting from displacement of well-consolidated rocks. An attempt to date fault gouge sample from Desamangalam, Kerala was recently carried out by examining the completely reset smaller grain fractions using the plateau method[6]. Arid to semi-arid climates are conducive for evaporite deposits and often result in crystallization of fibrous gypsum along the fault and fracture planes after the displacement culminates[7–9]. These fillings occur provided suitable conditions exist for the dissolution and precipitation of sulphate-rich brines to enter the extensional openings. ESR studies on the radiation-induced defects in gypsum crystals would enable to determine the amount of natural radiation dose that the samples have received after precipitation. The age estimated is the minimum age or the upper limit of the last movement. It is essential to mention that the age of gypsum crystals determined by any chronometric method would indicate only the age of its crystallization and not the faulting event as such. However, fibrous gypsums are known[8,9] to grow contemporaneously with the extensional openings. The present article discusses the studies on ESR dating of gypsum precipitated along the fault plane from Katrol Hill Range (KHR), Kachchh (Figure 1), essentially to demonstrate the robustness of the technique as a dating tool on fibrous gypsum precipitates in an arid region, and using it as an important material for Quaternary dating in order to provide an indirect age constraint. There exist no data on the time constraints of Quaternary deformation in Kachchh that are responsible for sculpturing the present-day topography.

*For correspondence. (e-mail: gmathew@iitb.ac.in)

ESR dating technique is usually grouped along with thermoluminescence and optically stimulated luminescence as trapped charge dating methods[10]. It allows the detection of paramagnetic centres and radicals, which are induced in minerals by ionizing radiation. Minerals are usually regarded as insulators and therefore show two energy levels where electrons might occur, the valence band and the conduction band. At the time of mineral formation, all electrons are in the ground state; however, with successive natural radiation (α, β, γ and cosmic radiation) electrons are transferred to the higher energy state. After a short period of diffusion, the excited electrons recombine with the holes or positively charged sites near the valence band. During crystallization minerals often accommodate some charge deficits or defect sites, which are capable of trapping electrons and form paramagnetic centres. This can be easily detected by ESR spectroscopy. The intensity of ESR signal is proportional to the trapped electrons at a given centre and therefore proportional to the strength of the radioactive field (dose rate).

An ESR age is determined by the following relationship:
Age = Accumulated dose (AD)/Dose rate (D).

AD is the radioactive dose that the sample has received since its formation. This value is determined by the additive dose method[5,6]. D is derived either by chemical analysis of radioactive elements U, Th and K or using gamma-ray spectroscopy or by alpha counting technique.

For the collection of samples, the surfaces were first thoroughly cleared and the upper surfaces were removed. Gypsum plates precipitated in 5–7 mm thick veins were carefully removed along the fault plane, and planes along bedding and fractures from the exposed bedrock. The surrounding samples were used for external dose measurements. Gypsum samples were cleaned in an ultrasonic bath, dried and then gently crushed in an agate mortar and sieved in order to separate fractions of 150–200 μm. The samples were then etched with 5% acetic acid to remove surface defects produced on account of crushing. They were then repeatedly washed and dried at room temperature. To determine accumulated dose, single aliquot measurements were carried out based on additive dose method using ^{60}Co source with a dose rate of 29 Gy/min. After irradiation, samples were annealed for 2 h at 100°C to allow fading of any short-lived ESR signals induced during laboratory-irradiation.

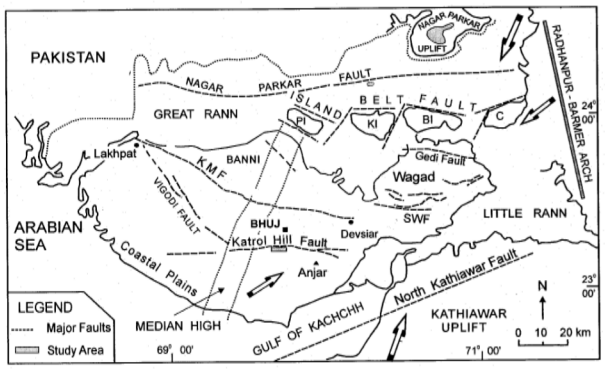

Figure 1. General tectonic map of Kachchh depicting the study area. Solid arrows indicate intrabasinal and regional stress directions (after Biswas and Khattri[18]).

ESR experiments were carried out using a Varian E-112 E line Century series X-band spectrometer, which utilizes 100 kHz field modulation. TCNE ($g = 2.00277$) was used as a standard for g-factor measurements. Typical power used is 2.0 mW. The dose rate estimation was done using the elemental composition. ZnS (Ag) thick source alpha counting was used to estimate U and Th, and K was analysed using ICP–AES. Radioactive disequilibrium and 10% water content were assumed in dose rate computations. It is considered that the effects of disequilibrium, if any, will be diluted as in most cases the potassium contributes up to the total dose. Internal dose rate is not taken into account due to small amount of sample. Dose rate is based on the external values of radioactive elements. The isotopic concentration is converted into dose rates using published table[11]. Powder X-ray diffraction studies were carried out to determine the purity of crystals using Phillips 1710.

The exposed normal fault plane containing the gypsum veins was collected from Satpura Dungar in the KHR front (Figures 1 and 2). The N35°E–S35°W trending fault dips at an angle of 48° cutting across intercalated ferruginous mudstone and shales. Apart from the samples of gypsum from the fault plane, samples were also collected from planes parallel to bedding and fracture fillings for comparative studies of the results. Samples collected were typical vein-filling satinspar variety of gypsum showing fibrous nature. They have typically grown perpendicular to the wall rock from either side of the openings, displaying several parallel layers of fibrous satinspar and all meet along a central parting plane (Figure 3 *a–f*). The fibrous gypsum crystals show increase in fibre width towards the centre and also towards the fracture wall. This characteristic textural evidence is manifestation of syntaxial growth, inward from the wall towards the centre and antiaxial growth from the centre towards the wall. Occasionally, mudstone and shale chips derived from the fracture-wall rock during fracture opening are observed in between two crystals and also along the central parting plane (Figure 3 *a*). The fibrous gypsum crystals along the fault plane show growth perpendicular to the fracture walls. Along the parting planes, the fault-plane gypsum crystals show zones of curved sigmoidal features with good optical continuity of the curved area (Figure 3 *c* and *d*). The gypsum crystals from fracture plane cutting across bedding planes also show occasional zones of curving of the fabric, but lack optical continuity indicating minor movements after crystallization (Figure 3 *e* and *f*).

Lack of optical continuity due to two generations of vein fillings is, however, not ruled out.

Altogether five samples of gypsum from fault plane (GY_F1a–d) (Figure 2) and one each from bedding (GY_B1) and fracture plane (GY_C1) were analysed (Table 1). The typical ESR spectra of gypsum are shown in Figure 4. GY_F1 fault-plane gypsums are composed of purely gypseous material with complete absence of impurities, as can been seen from the powder X-ray diffraction analysis with peaks at 7.61, 3.07, 2.87 and 2.66 Å (Figure 5).

Based on single crystal studies on gypsum crystals, four main types of centres were identified and termed as G1 ($g = 2.004$), G2 ($g = 2.008$), G3 ($g = 2.003$) and G4 ($g = 1.999$)[12]. The G1 centre is attributed to SO_3^- radical. Single crystal studies reveal that it has isotropic g-factor with $g = 2.0028$–2.0042. The G2 centre is assigned to CO_3^- radical, which consists of two magnetically non-equivalent sites having a g-tensor of rhombic symmetry with $g_{zz} = 2.0192$, $g_{xx} = 2.0084$ and $g_{yy} = 2.0058$. The G3 centre is attributed to CO_2^- radical and has orthorhombic symmetry with $g_{zz} = 1.9973$, $g_{xx} = 2.0029$ and $g_{yy} = 2.0027$. The G4 centre is assigned to (O_2H) centre[12,13].

Figure 4 represents the powder ESR spectra of gypsum precipitates from the fault plane. Gypsum spectra before additive irradiation reveal signals associated with Mn^{2+} hyperfine lines at $g = 2.012$ and $g = 1.996$, due to forbidden transitions. Additive irradiation shows enhancement of the signals G1, G2 and G3. The mean life of the signal at $g = 2.004$ is 10^{12} yrs, whereas the signal at $g = 2.008$ is more stable than the former[14,15]. ESR studies on gypsum sands by Yijian *et al.*[13] showed that the AD values from $g = 2.008$ are consistent with the added dose, but the $g = 2.004$ signal yielded an AD value up to one order of magnitude higher. Hence, it appears that in gypsum the only signal suitable for dating is at $g = 2.008$. ESR dating studies on gypsum precipitates from San Andreas Fault[16] also suggested the use of $g = 2.008$ signal for AD measurement. The study however, gave an age approximately twice that of the last great movement in the year 1857. The discrepancy between the ESR age and the historical record of the displacement was attributed to the influence of internal alpha dose and contamination with older gypsum particles.

Figure 2. Satinspar gypsum along fault plane cutting across mudstone and shale sequence at Satpura Dungar. Sample positions collected for ESR dating along fault plane are represented. Scale: closed circle enclosing pen (6″). Approximate displacement along normal fault is 1.0 m.

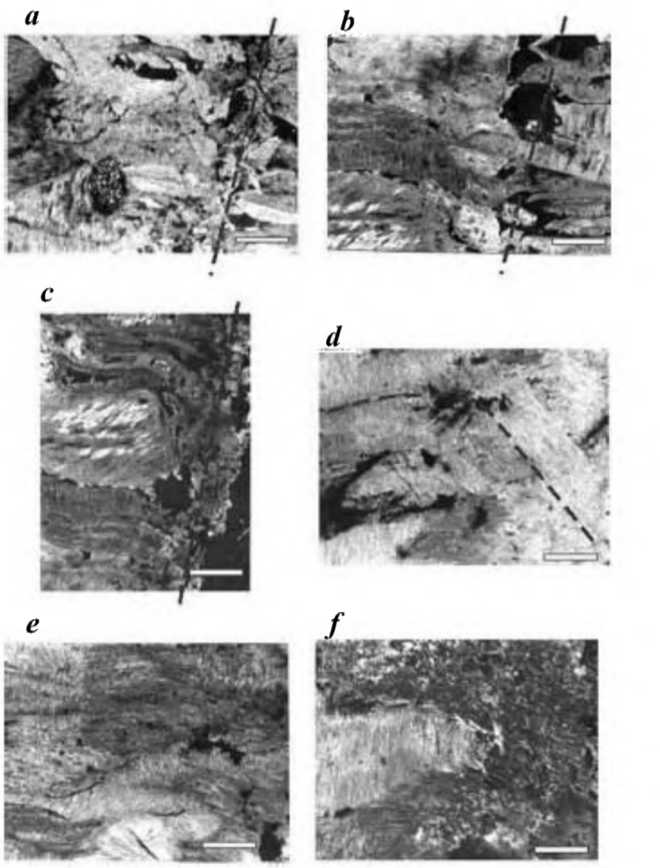

Figure 3. Microfabrics of fibrous gypsum (photos under crossed nicols; scale bar = 1 mm). ***a***, Growth of fibrous gypsum perpendicular to wall rock with occasional presence of chips of mudstone in between fibres and along parting plane. Dashed line represents parting plane. ***b***, Another representation of parting planes with interspersed growth of fibrous gypsum from both ends of wall rock. ***c***, Curved fault plane gypsum crystals along parting planes showing optical continuity. ***d***, Curved fabrics of gypsum crystals with optical continuity. ***e***, Increasing width of gypsum fibres towards centre and curving along parting plane with lack of optical continuity. ***f***, Curving and lack of optical continuity of gypsum fibres along fracture planes.

Table 1. ESR age details of satinspar gypsum along fault, bedding and fracture plane

Sample code	Location	U (ppm)	Th (ppm)	K (wt%)	Internal dose D_I (Gy/ka)	U (ppm)	Th (ppm)	K (wt%)	External dose D_E (Gy/ka)	Total dose $D_T = D_I + D_E$ (Gy/ka)	AD (Gy)	Age (ka) AD/D_T
GY_F1a	Fault	0.32 ±	1.80 ±	0.96 ±	0.57	4.45 ±	7.80 ±	0.22 ±	1.814	1.87 ±	130 ±	69.5 ±
	plane	0.11	0.41	0.04		1.15	3.95	0.01		0.37	12	15
GY_F1b	Fault	0.49 ±	1.86 ±	0.92 ±	0.57	4.27 ±	7.63 ±	0.21 ±	1.760	1.82 ±	121 ±	66.4 ±
	plane	0.17	0.61	0.04		1.01	3.81	0.01		0.35	11	14
GY_F1c	Fault	0.50 ±	1.89 ±	0.95 ±	0.59	4.53 ±	7.80 ±	0.22 ±	1.845	1.90 ±	140 ±	73.6 ±
	plane	0.18	0.64	0.04		1.12	3.95	0.01		0.31	14	19
GY_F1d	Fault	0.51 ±	1.87 ±	0.96 ±	0.65	4.60 ±	7.95 ±	0.20 ±	1.860	1.92 ±	144 ±	75 ±
	plane	0.18	0.65	0.04		1.23	3.75	0.01		0.37	15	19
GY_B1	Bedding	0.55 ±	1.62 ±	0.92 ±	0.57	4.15 ±	5.43 ±	0.20 ±	1.744	1.64 ±	605 ±	335 ±
	plane	0.19	0.82	0.04		1.00	2.26	0.01		0.20	48	55
GY_C1	Fracture	0.64 ±	2.62 ±	0.40 ±		2.41 ±	6.92 ±	0.20 ±	1.311	1.35 ±	412 ±	306 ±
	plane	0.29	1.02	0.01	0.41	0.66	2.07	0.01		0.21	31	42

D_I, Internal dose rate; D_E, External dose rate and D_T, Total dose rate.

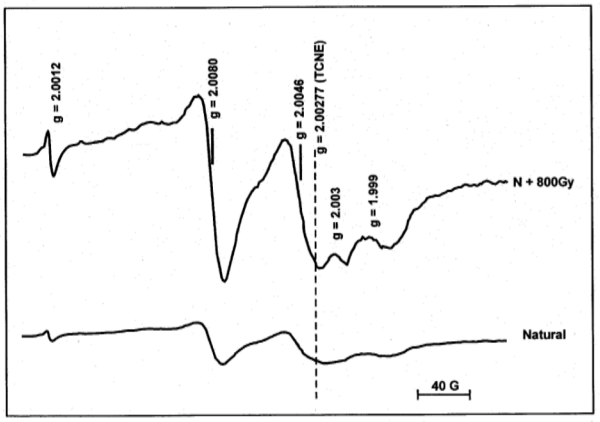

Figure 4. ESR spectra of natural and irradiated gypsum aliquots from fault plane. Peak-to-peak height of $g = 2.008$ is used for AD estimation.

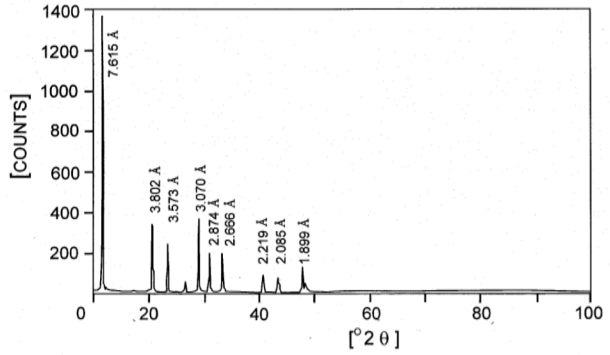

Figure 5. Powder X-diffractogram of satinspar gypsum indicating absence of any contamination with other mineral phases.

Figure 6 represents AD plot of the fault-plane-filling gypsum. In the AD plots, both $g = 2.0080$ and $g = 2.0046$ signal growth are shown, but for the age calculations only 2.0080 is used as it is a more thermally stable centre. AD values of gypsum in the fault plane were estimated from four different positions from top to bottom (Figure 2). The age of gypsum mineralization that succeeds the event of rupture along the fault plane is the mean AD obtained out of the four samples analysed (Table 1). The variation in AD values from different positions is attributed probably to the variation in internal dose rates. Errors in AD estimation are determined using least square refinement method. The bedding plane gypsum shows AD of 605 Gy, which is estimated based on the average of four aliquots to correct for the spectrometer variation. Similarly, the fracture plane gypsum shows AD 412 of Gy. Table 1 shows the estimated U, Th and K concentrations, annual dose rates and ESR ages of gypsum precipitates.

Microfabric studies on gypsum precipitates indicate the absence of wavy extinctions and presence of optical continuity. This indicates continuous growth of fibrous gypsum and absence of significant post-growth movements along the fault plane, whereas the fracture planes cutting across the bedding planes do show evidences of curving of elongate fibres (Figure 3 *c* and *d*), indicating post-growth shear movements. Variation in the size of gypsum crystals along the bedding plane is attributed to changes in the rate of crystal growth or variation in fracture opening, or could also be due to later generation vein-filling gypsum material. The latter described textures are, however, not observed in the fault plane, deducing that the fracture opening and crystallization were probably contemporaneous, which resulted in crystallization of elongate crystal fibres. Simultaneous crystal growth and fracture opening along the fault plane is further supported by the occasional presence of mudstone and shale chips of the host rock as inclusions within the gypsum crystals (Figure 3 *a*) and growth of fibres perpendicular to the wall (Figure 3 *a–f*). The above-mentioned observations also suggest that the satinspar gypsum along the fault plane is exclusively primary in origin and not a product of hydration of earlier anhydrite veins.

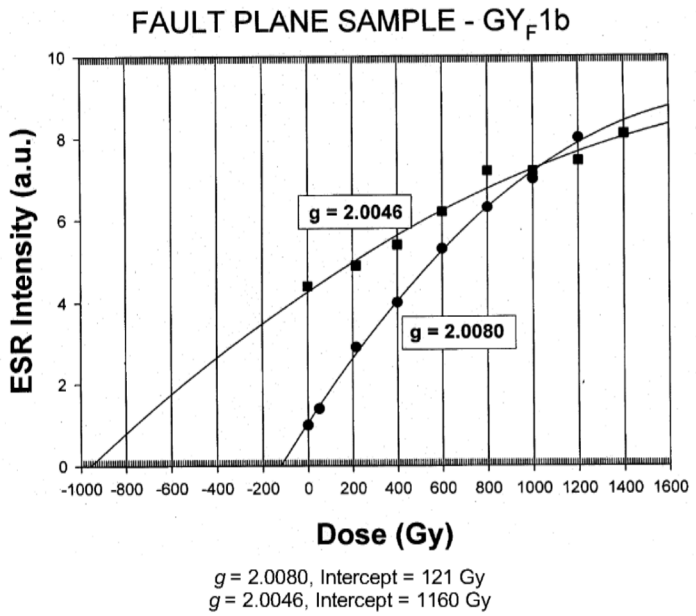

Figure 6. AD plot of fault-plane gypsum using additive dose technique for ESR signal at $g = 2.0046$ and $g = 2.0080$. Intercept of line with $g = 2.0080$ is used for estimation of AD for all samples studied.

The Kachchh basin consists of considerable amount of calcium sulphate and halite deposits all along the KHR and also huge deposits in Banni and Rann area, formed typically under conditions where evaporation exceeds precipitation. The satinspar vein deposit occupying the extensional openings is on account of the dissolution of earlier evaporite deposits. The present-day exposed section containing the gypsum crystals under study was under the subsurface earlier when sulphate-rich brines could enter the fractures as fillings and then grow perpendicular to the wall of the openings.

The basic structural framework of Kachchh represents a rift basin of Late Triassic–Early Jurassic age[17,18]. This rift basin is now under the influence of compressional stress regime due to ongoing collision of Indian and Eurasian plates. The landscape thus consists of complex structural patterns marked by uplifts and low-lying depressions. Uplifts are mainly confined along the major sub-parallel longitudinal faults (Figure 1), e.g. the Katrol Hill Fault (KHF), Kachchh Mainland Fault, Banni Fault and Island Belt Fault[18].

The altitude of the KHR varies from about 148 to 348 m and is flanked to its north by the KHF (Figure 1), which marks the major drainage divide in the Kachchh Mainland. Uplift and compressional deformation of this range along KHF has controlled the development of numerous north- and south-flowing rivers[19]. Intense asymmetric folding of the Mesozoic and Tertiary bedrock has given rise to the range with north-facing steep forelimb and gentle back limb dipping due south. The uplifts in the form of asymmetrical fold and monoclinal flexures along the bounding faults are a complex manifestation of fault-related folding. Folding of Middle Pleistocene milolite rocks clearly suggests that deformation has continued during Upper Pleistocene to Holocene[20]. The extensional openings that are observed along the limb/hinge throughout the Kachchh region, have been inferred to be due to the ongoing compressional tectonism experienced by the Kachchh basin[21]. This deformation is also considered to be compressional, thin-skinned type and could be associated with fault-related folding, which resulted in the slow uplift and early dissolution of evaporite deposits resulting in initial fillings along the bedding plane around 335 ka, based on the ESR age of bedding-plane gypsum (GY_B1). This is followed by the development of irregular extensional opening cutting across the bedding plane and gypsum filling around 306 ka, based on ESR age of fracture vein (GY_C1). The final stage was marked by continued progressive uplift resulting in several normal faults perpendicular to the compressive stresses across the KHR. The normal faulted extensional openings provided favourable sites for fibrous gypsum growth as seen in the present study from one of the exposed section (Figure 2). Gypsum ESR age of fault plane (GY_F1b) indicates that this happened sometime close to 70 ka. The continued compressive stresses resulted in active uplift along the KHR backlimb, exposing the study area to its present topography.

The above observations of active uplift during Late Quaternary observed in KHR based on ESR ages are further corroborated by the luminescence ages on the channel-fill deposits over the incised bed rocks[22]. This study revealed that the initiation of river incision by the antece-

dent drainages is as young as ~12 ka, incising over 25 m of its own bedrocks. The present study, although based on ESR chronometry studies from single-fault-plane gypsum, provides some important time constraints on the Quaternary deformation over KHR. This, however, needs to be supported by more such data in order to understand the neotectonic activity of the region.

1. Bar, M., Kolodny, Y. and Bentor, U. K., Dating of faults by fission track dating of epidotes. An attempt. *Earth Planet. Sci. Lett.*, 1974, **22**, 157–166.
2. Eyal, Y., Kaufman, A. and Matthews, M, B., Use of $^{Th}230/U$ ages of striated carnotites for dating fault displacements. *Geology*, 1992, **20**, 829–832.
3. Karlik, M., Clauer, N., Holnsteiner, R., Huemer, H. and Kappel, F., Recurrent fault activity in the Grimsel Test Site: revealed by Rb–Sr, K–Ar and tritium isotope techniques. *J. Geol. Soc. London*, 1992, **149**, 293–301.
4. Singhvi, A. K., Banerjee, D., Pande, K, Gogte, V. and Valdiya, K. S., Luminescence studies on neotectonic events in south Central Kumaun Himalaya – A feasibility study. *Quat. Sci. Rev.*, 1994, **13**, 595–600.
5. Ikeya, M., Miki, T. and Tanaka, T., Dating of a fault by electron spin resonance on interfault materials. *Science*, 1982, **215**, 1392–1393.
6. Gundu Rao, T. K., Rajendran, C. P., Mathew, G. and John, B., Electron Spin Resonance dating of fault gouge from Desamangalam, Kerala: Evidence for Quaternary movement in Palghat-shear zone. *Proc. Indian Acad. Sci.* (*Earth Planet. Sci.*), 2002, **111**, 103–113.
7. Machel, Hans. G., Fibrous gypsum and fibrous anhydrite in veins. *Sedimentology*, 1985 **32**, 443–454.
8. Gaustavson, T. C., Hovorka, S. and Dutton, A. R., Origin of satinspar veins in evaporate basin. *J. Sediment. Res.*, 1994, **64**, 88–94
9. Tabakh, M., Schreiber, B. C. and Warren, J. K., Origin of fibrous gypsum in the Newark rift basin, eastern North America. *J. Sediment. Res.*, 1998, **8**, 1, 88–99.
10. Ikeya, M., *New Application of Electron Spin Resonance: Dating, Dosimetry and Microscopy*, World Scientific, 1993, p. 499.
11. Adamiec, G. and Aitken, M., Dose rate conversion factors: Update. *Ancient TL*, 1998, **16**, 37–50.
12. Kasuya, M., Brumby, M. S. and Chappell, J., ESR signal in gypsum single crystals: implications for ESR dating. *Nucl. Tracks Radiat. Meas.*, 1991, **18**, 329.
13. Yijian, C., Arakel, A. V. and Jinfen, L., Investigation of sensitive signals due to gamma-ray irradiation of chemical precipitates. A feasibility study for ESR dating of gypsum, phosphate and calcrete deposits. *Int. Radiat. Isot.*, 1989, **40**, 1163–1170.
14. Nambi, K. S. V. and Higashimura, T., TL and EPR studies on natural CaF_2 after heavy gamma irradiation. *Radiat. Effects*, 1971, **10**, 197–199.
15. Nambi, K. S. V., ESR and TL studies on marine gypsum, *PACT*, 1982, **6**, 314.
16. Ikeda, S. and Ikeya, M., Electron spin resonance (ESR) signals in natural and synthetic gypsum: An application of ESR to the age estimation of gypsum precipitates from the San Andreas Fault. *J. Appl. Phys.*, 1992, **31**, L 136–138.
17. Biswas, S. K., Regional tectonic framework, structure and evolution of the western marginal basins of India. *Tectonophysics*, 1987, **135**, 307–327.
18. Biswas, S. K. and Khattri, K. N., A geological study of earthquakes in Kutch, Gujarat, India. *J. Geol. Soc. India*, 2002, **60**, 131–142.
19. Malik, J. N., Sohoni, P. S., Merh, S. S. and Karanth, R. V., Active tectonic control on alluvial fan architecture along the Kachchh Mainland Hill Range, western India. *Z. Geomorphol.*, 2001, **45**, 80–100.
20. Sohoni, P. S., Malik, J. N., Merh, S. S. and Karanth, R. V., Active tectonics astride Katrol Hill Zone, Kachchh, W. India. *J. Geol. Soc. India*, 1999, **53**, 579–586.
21. Sohoni, P. S. and Karanth, R. V., Jointing and fracturing characteristics of Central Kachchh Mainland. *J. Geol. Soc. India*, 2003, **61**, 673–684.
22. Mathew, G. and Singhvi, A. K., Luminescence chronometry of tectonic landforms in Kachchh, W. India: Evidences of lateral eastward propagation of the Kachchh Mainland Fault. INQUA, Nevada, USA, 2003.

ACKNOWLEDGEMENTS. Financial support provided by the Department of Science and Technology, New Delhi to R.V.K. is acknowledged. We thank the anonymous referees for their critical comments and suggestions that greatly improved the manuscript.

Received 18 October 2003; revised accepted 30 July 2004